Electronic Supplementary Information (ESI)

Highly efficient electroluminescence from evaporation- and solution-processable orange-red thermally activated delayed fluorescence emitters

Binyan Wang,[a] Hannan Yang,[b] Yaxing Zhang,[a] Guohua Xie,*[c] Huijuan Ran,[a] Tao Wang,[d] Qiang Fu,[e] Yitao Ren,[b] Ning Sun,*[b] Guangtao Zhao,[a] Jian-Yong Hu,[a] Qiang Wang*[a]

[a] *Key Laboratory of Applied Surface and Colloid Chemistry, National Ministry of Education, Shaanxi Key Laboratory for Advanced Energy Devices, Shaanxi Engineering Lab for Advanced Energy Technology, School of Materials Science and Engineering, Shaanxi Normal University, Xi'an 710119, China*

[b] *Department of Physics, Center for Optoelectronics Engineering Research, Yunnan University, Kunming 650091, China*

[c] *Department of Chemistry, Hubei Key Lab on Organic and Polymeric Optoelectronic Materials, Wuhan University, Wuhan 430072, China*

[d] *Key Laboratory of Applied Surface and Colloid Chemistry, National Ministry of Education, School of Chemistry and Chemical Engineering, Shaanxi Normal University, Xi'an 710119, China*

[e] *Department of Electrical and Computer Engineer, University of California at Davis, Davis, CA 95616, USA*

* Corresponding authors.

E-mail: qiangwang@snnu.edu.cn; ning.sun@ynu.edu.cn; guohua.xie@whu.edu.cn

Materials and general methods

All chemicals, reagents, and solvents were used as received from commercial sources without further purification. All reactions were carried out under nitrogen and anhydrous conditions unless noted otherwise. The syntheses of 7,10-dibromo-2,3-dicyanopyrazino phenanthrene, 3,6-diphenyl-9*H*-carbazole, and 3,6-bis(4-(diphenylamino)phenyl)-9*H*-carbazole followed the procedures described in the previous reports.[1-3]

^{1}H NMR (400 MHz) and ^{13}C NMR (100 MHz) spectra were measured on a Bruker Ascend 400 spectrometer using $CDCl_3$ as a solvent and the spectral data were reported in ppm relative to tetramethylsilane (TMS) as an internal standard. Molecular weights were measured with a Bruker Autoflex III MALDI-TOF mass spectrometer. Elemental analyses of carbon, hydrogen, and nitrogen were performed on a Vario EL III microanalyzer. Thermogravimetric analysis (TGA) was undertaken with a TA instrument Q600 at a scanning rate of 10 ℃/min under nitrogen atmosphere. Differential scanning calorimetry (DSC) was performed on a Mettler Toledo DSC1 STARe system with nitrogen flow at 20 mL/min. Samples were preheated to above their melting points, and then cooled down to –30 ℃ at –100 ℃/min before the second heating and cooling scans were recorded at 20 ℃/min. UV-vis absorption spectra were recorded on a Perkin-Elmer Lambda-900 spectrophotometer. PL spectra were measured on a Hitachi F-7000 fluorescence spectrophotometer and phosphorescence spectra at 77 K were recorded on a Perkin-Elmer LS 50B spectrofluorometer. The absolute PL quantum yields were measured using a Hamamatsu C9920-02G integrating sphere

system coupled with a 150 W xenon lamp and a PMA-12 photonic multichannel analyzer. The transient PL decay measurements were performed using an Edinburgh Instruments FLS980 spectrometer. CV was carried out using nitrogen-purged anhydrous THF for the reduction and dichloromethane (DCM) for the oxidation scan at room temperature with a CHI voltammetric analyzer. Tetrabutylammonium hexafluorophosphate ($TBAPF_6$) (0.1 M) was used as the supporting electrolyte. The conventional three-electrode configuration consists of a glassy carbon working electrode, a platinum wire counter electrode, and a saturated calomel reference electrode (SCE) with ferrocene/ferrocenium (Fc/Fc^+) as the internal standard. The working electrode surface was previously polished with alumina slurry on a micro cloth. The dilute sample solutions exhibit reduction and oxidation scans against the Ag/AgCl reference electrode. Cyclic voltammograms were obtained at a scan rate of 100 mV/s. The reduction and oxidation potentials, $E_{1/2}$(red) and $E_{1/2}$(oxd), relative to (Fc/Fc^+) were used to calculate the LUMO and HOMO levels as $-4.80-qE_{1/2}$(red) eV and $-4.80-qE_{1/2}$(oxd) eV, respectively, where q is electron charge. The atomic force microscopy (AFM) was conducted on a Bruker Dimension ICON. All calculations were performed utilizing the Gaussian 09 program package. Geometry optimizations were conducted in the framework of the density functional theory (DFT) at the B3LYP level. The 6-31G(d,p) basis set was used for all the elements. The molecular orbitals were visualized using Gaussview.

Equations for calculation of rate constants

$$k_r = \Phi_p k_p + \Phi_d k_d \qquad (1)$$

$$k_{nr} = \frac{1 - \Phi_{PL}}{\Phi_{PL}} k_r \quad (2)$$

$$k_{ISC} \approx \frac{\Phi_d}{\Phi_p \Phi_{PL}} k_r \quad (3)$$

$$k_{RISC} \approx \frac{k_p k_d}{k_r} \Phi_{PL} \quad (4)$$

Device fabrication and characterization

The fabricated devices were grown on clean glass substrates pre-coated with a 180-nm thick layer of ITO with a sheet resistance of 15−20 Ω/sq. The ITO surface underwent a wet-cleaning course in an ultrasonic solvent bath, and then was dried at 120 ℃ before the UV-Ozone treatment for 20 min. For the vacuum deposited devices, all layers were grown in succession by thermal evaporation at a pressure below 5×10^{-4} Pa without breaking vacuum. The thickness of each layer was determined by a quartz thickness monitor. For the solution-processed devices, a 40 nm thick PEDOT:PSS layer used as a hole- injecting layer was spin-coated on the ITO substrate and then baked inside the glove-box at 120 °C for 10 min. The EML was prepared by spin-coating from chlorobenzene solution on top of the PEDOT:PSS layer. The electron-transporting, electron-injecting, and cathode layers were sequentially deposited in a vacuum chamber. Current–brightness–voltage characteristics were measured using Keithley source measurement units (Keithley 2400 and Keithley 2000) with a calibrated silicon photodiode. The EL spectra were measured using a SpectraScan PR650 spectrophotometer. External quantum efficiencies were calculated from the luminance, current density, and EL spectrum, assuming a Lambertian distribution. All the measurements were carried out in an ambient atmosphere.

Table S1 Summary of photophysical rate constants for DDPhCz-DCPP and DDTPACz-DCPP in doped CBP films

Compound	k_r (10^7 s^{-1})	k_{nr} (10^7 s^{-1})	k_{ISC} (10^7 s^{-1})	k_{RISC} (10^5 s^{-1})
DDPhCz-DCPP	0.56	0.29	3.46	3.24
DDTPACz-DCPP	1.25	1.11	3.59	2.60

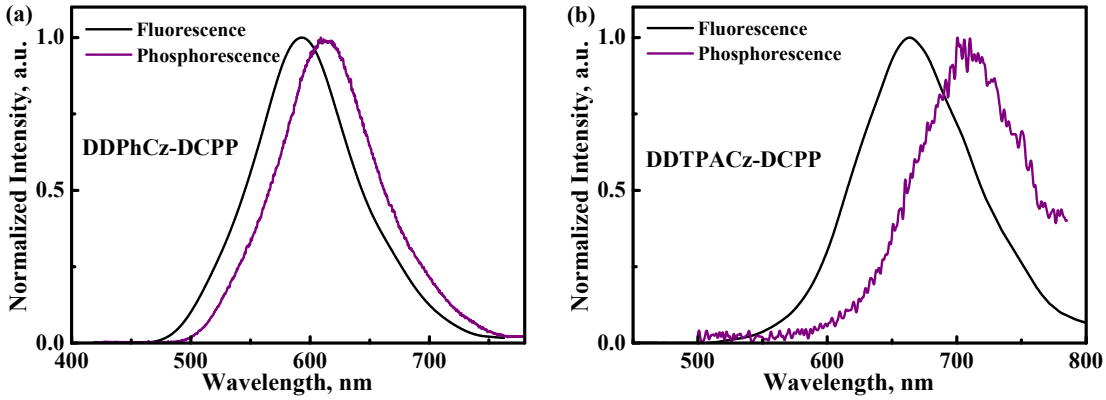

Fig. S1 Fluorescence and phosphorescence spectra for (a) DDPhCz-DCPP and (b) DDTPACz-DCPP in doped CBP films at a concentration of 10 wt%.

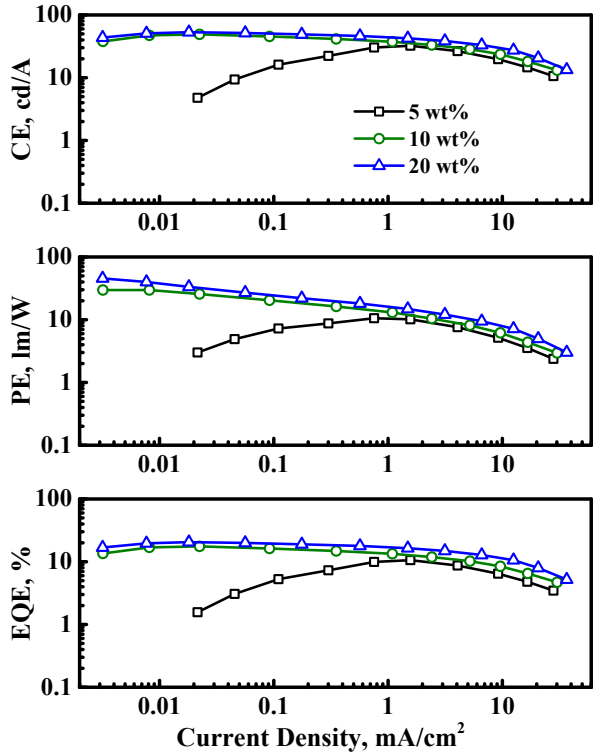

Fig. S2 Current efficiency (CE), power efficiency (PE), and external quantum efficiency (EQE) as a function of current density for the solution-processed OLEDs based on DDPhCz-DCPP.

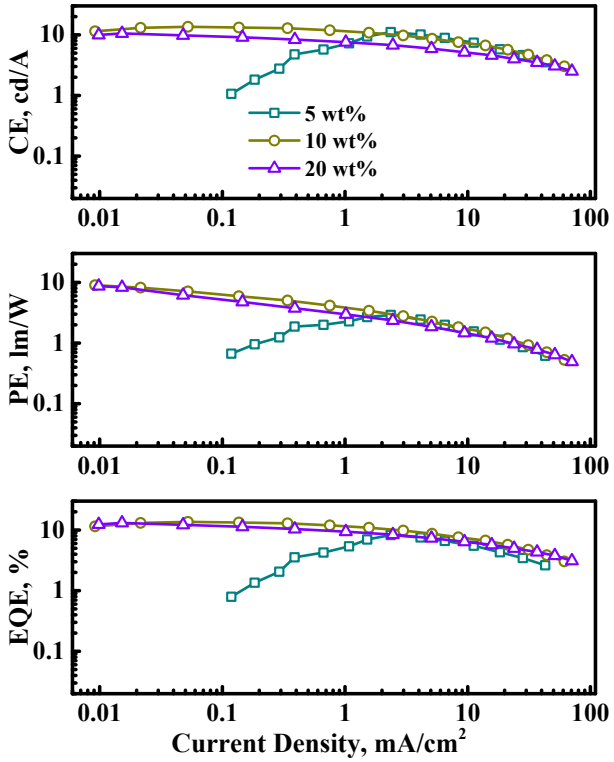

Fig. S3 Current efficiency (CE), power efficiency (PE), and external quantum efficiency (EQE) as a function of current density for the solution-processed OLEDs based on DDTPACz-DCPP.

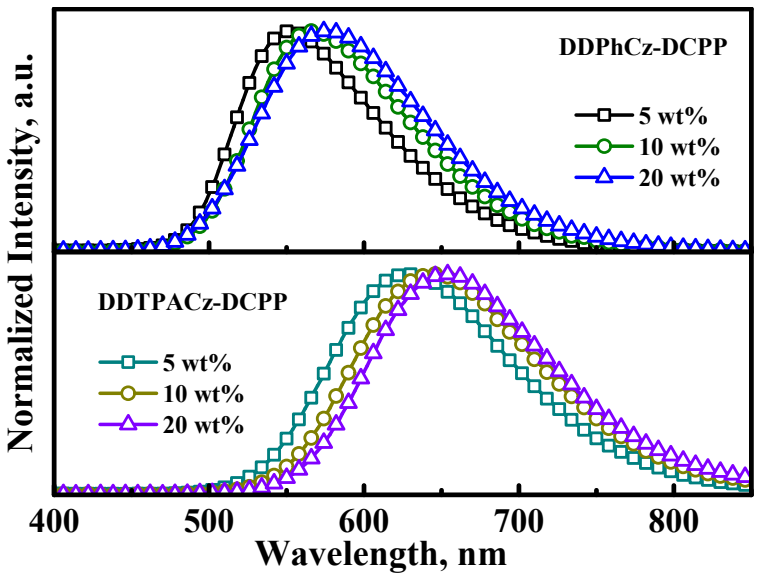

Fig. S4 EL spectra of the solution-processed OLEDs.

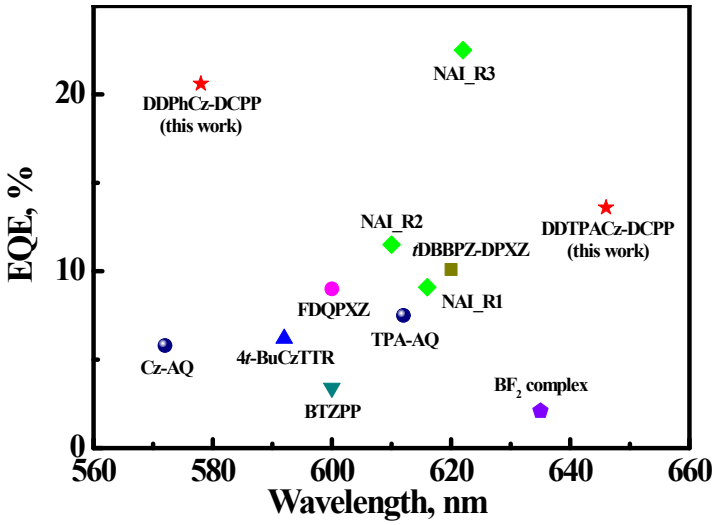

Fig. S5 Comparison of solution-processed orange-red TADF OLEDs reported in the literature.[1-7]

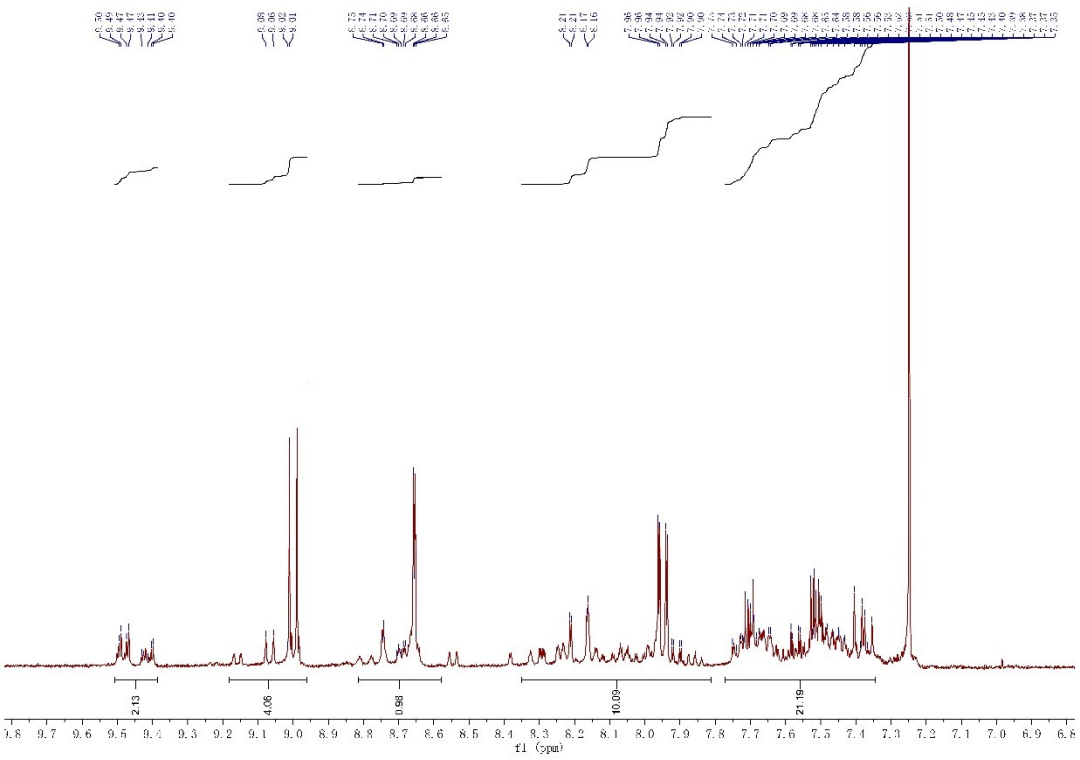

Fig. S6 ^{1}H NMR spectrum of DDPhCz-DCPP in $CDCl_3$.

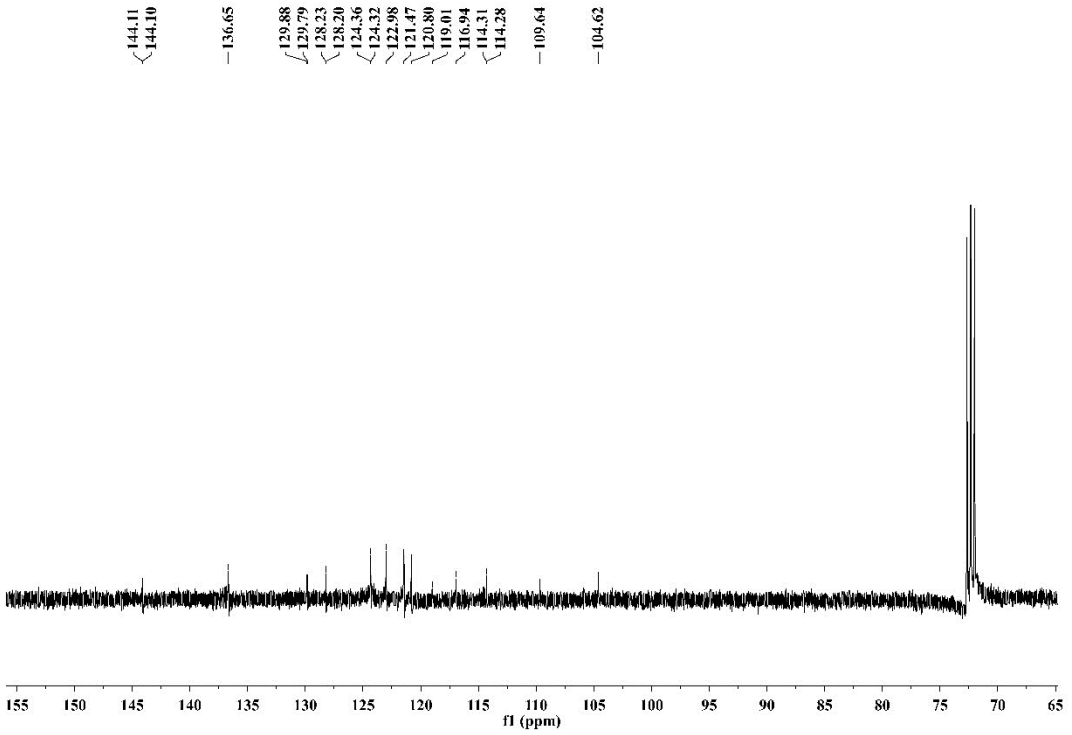

Fig. S7 ^{13}C NMR spectrum of DDPhCz-DCPP in $CDCl_3$.

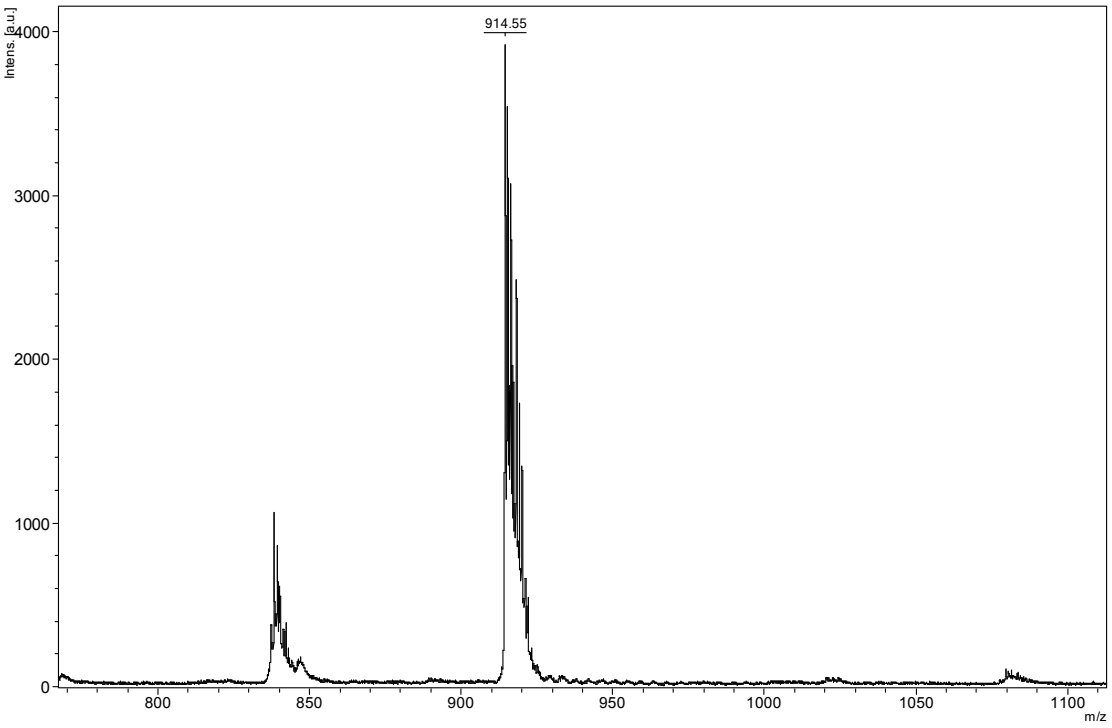

Fig. S8 MALDI-TOF-MS spectrum of DDPhCz-DCPP.

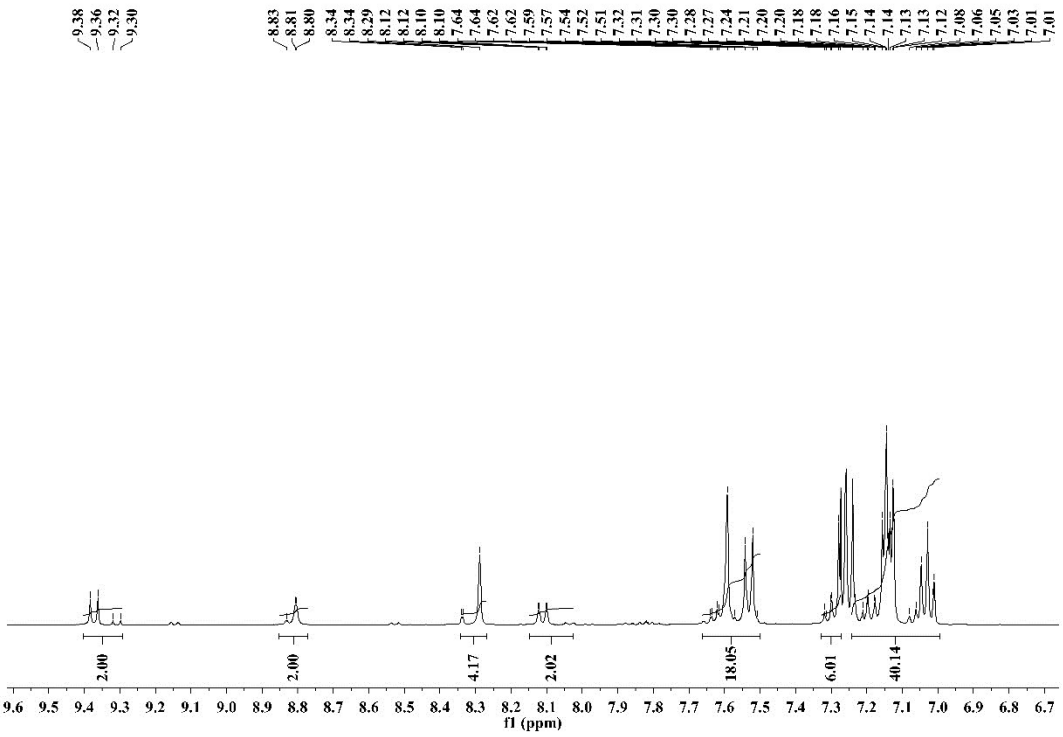

Fig. S9 ^{1}H NMR spectrum of DDTPACz-DCPP in $CDCl_3$.

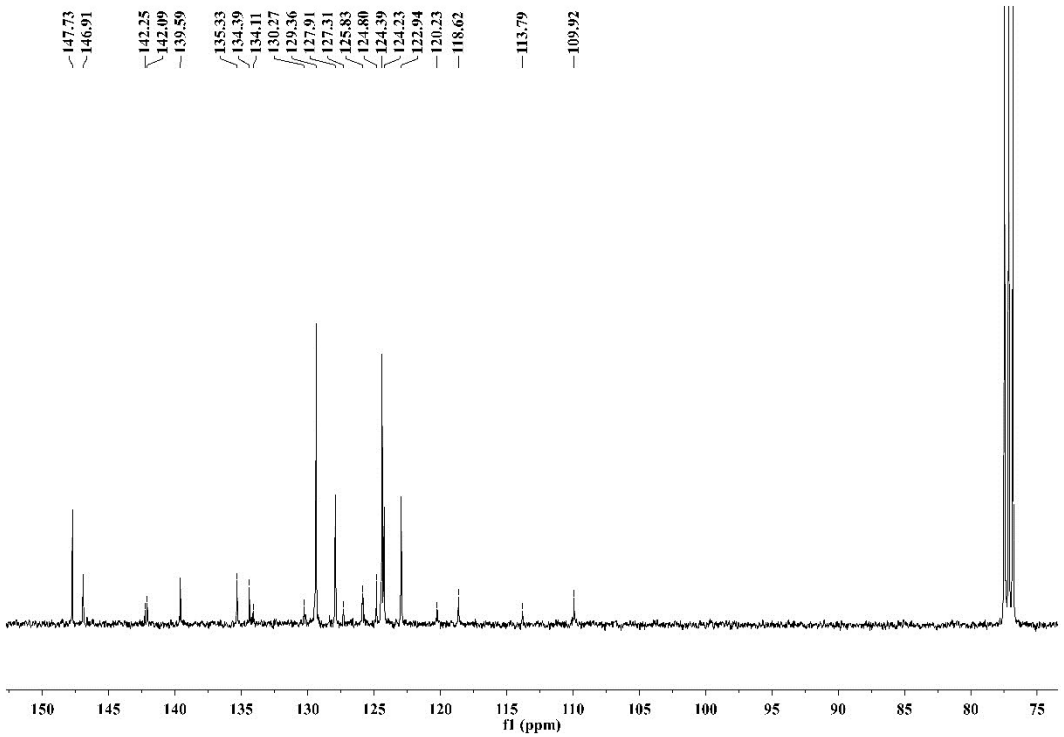

Fig. S10 ^{1}H NMR spectrum of DDTPACz-DCPP in $CDCl_3$.

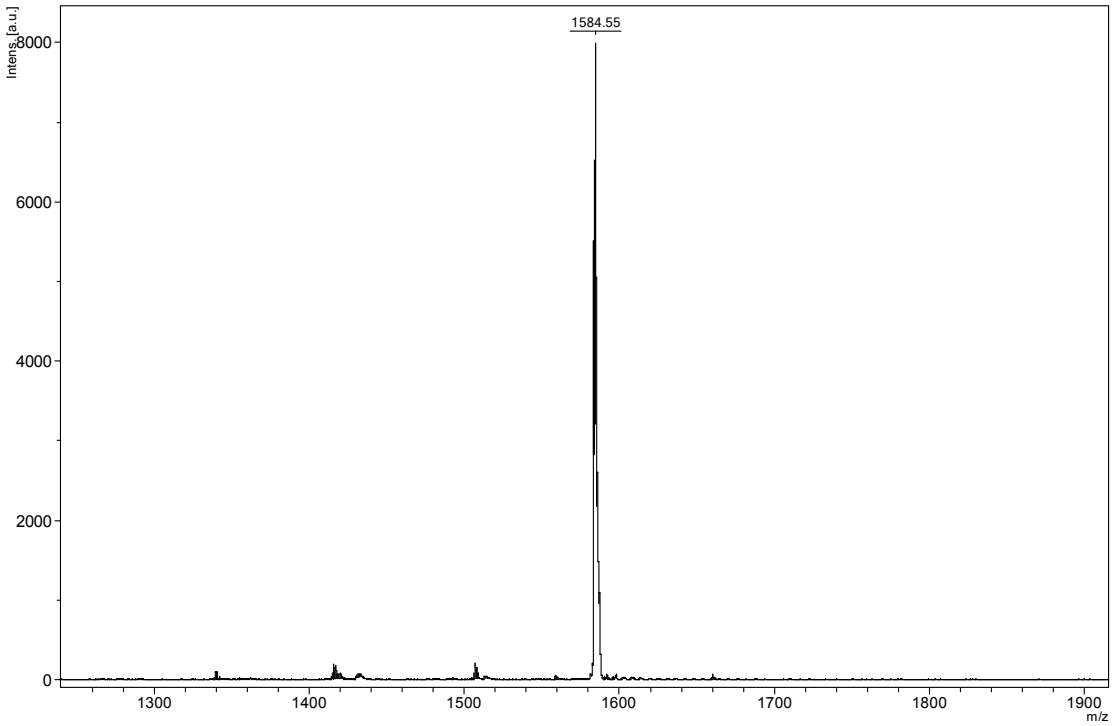

Fig. S11 MALDI-TOF-MS spectrum of DDTPACz-DCPP.

References

[1] L. Yu, Z. Wu, G. Xie, C. Zhong, Z. Zhu, H. Cong, D. Ma and C. Yang, *Chem. Commun.*, 2016, **52**, 11012–11015.

[2] A. D'Aleo, M. H. Sazzad, D. H. Kim, E. Y. Choi, J. W. Wu, G. Canard, F. Fages, J. C. Ribierre and C. Adachi, *Chem. Commun.*, 2017, **53**, 7003–7006.

[3] H. Bin, Y. Ji, Z. Li, N. Zhou, W. Jiang, Y. Feng, B. Lin and Y. Sun, *J. Lumin.*, 2017, **187**, 414–420.

[4] X. Li, K. Wang, Y.-Z. Shi, M. Zhang, G.-L. Dai, W. Liu, C.-J. Zheng, X.-M. Ou and X.-H. Zhang, *J. Mater. Chem. C*, 2018, **6**, 9152–9157.

[5] Y. Zhou, M. Zhang, J. Ye, H. Liu, K. Wang, Y. Yuan, Y.-Q. Du, C. Zhang, C.-J. Zheng and X.-H. Zhang, *Org. Electron.*, 2019, **65**, 110–115.

[6] J. X. Chen, W. W. Tao, Y. F. Xiao, K. Wang, M. Zhang, X. C. Fan, W. C. Chen, J. Yu, S. Li, F. X. Geng, X. H. Zhang and C. S. Lee, *ACS Appl. Mater. Interfaces*, 2019, **11**, 29086–29093.

[7] W. Zeng, T. Zhou, W. Ning, C. Zhong, J. He, S. Gong, G. Xie and C. Yang, *Adv. Mater.*, 2019, **31**, 1901404.